Indonesian Journal of Material Research
***e*-ISSN: 2987-1654**
Vol. 2, No. 3, November 2024

Indonesian Journal of MATERIAL RESEARCH

Research Paper

Carbon-Based Adsorbents from Biochar and Microcrystalline Cellulose for Phenol Removal in Aqueous Solutions

Novie Juleanti[1*], Patimah Mega Syah Bahar Nur Siregar[1], Erni Salasia Fitri[1]

[1] *Research Centre of Inorganic Materials and Coordination Complexes, Universitas Sriwijaya, Palembang, South Sumatera, 30139, Indonesia*
[*]**Corresponding author**: novie.lea13@gmail.com

Abstract
This study investigates the adsorption characteristics of phenol on rice husk biochar (BC) and microcrystalline cellulose (MC), with a focus on their structural, kinetic, isotherm, and thermodynamic properties. XRD and FTIR analyses reveal that BC and MC possess similar carbon-based structures. Nitrogen adsorption-desorption isotherms highlight BC's higher surface area and pore volume, which likely contribute to its superior adsorption performance. Adsorption kinetics are best described by the PSO model, indicating chemisorption as the rate-limiting step. Isotherm studies show that the Langmuir model provides a better fit, suggesting monolayer adsorption on homogeneous surfaces. Thermodynamic parameters indicate that phenol adsorption onto BC is endothermic and spontaneous, with adsorption capacity increasing with temperature, while MC shows minimal temperature sensitivity. The adsorption capacity of phenol using BC and MC was obtained as 28.50 mg/g and 13.25 mg/g, respectively. The reusability tests reveal that BC retains significant adsorption capacity over multiple cycles compared to MC. Overall, BC is identified as a more efficient and reusable adsorbent for phenol removal in aqueous solutions.

Keywords
Adsorbent, Biochar, Microcrystalline Cellulose, Adsorption, Phenol

Received: 13 July 2024, Accepted: 19 November 2024
https://doi.org/10.26554/ijmr.20242345

1. INTRODUCTION

Phenol (C_6H_5OH) is an aromatic compound characterized by its weak acidity, and it finds extensive application across various industries, including petrochemical, agricultural, pharmaceutical, and coking sectors, among others (Neziri and Duranoğlu, 2024; Zubir et al., 2024). Phenolic compounds find extensive application in the manufacturing of pesticides, dyes, cosmetics, disinfectants, and plastic products (Wu et al., 2024). Phenol presents a significant risk to all living organisms, including humans and aquatic life, due to its high toxicity even at minimal exposure levels. Phenol poses significant hazards to human respiratory health, vision, reproductive capabilities, and may contribute to the development of cancer. Phenol and its derivatives represent significant organic pollutants of concern, attributed to their bioaccumulative nature and a range of detrimental effects, which encompass carcinogenic, mutagenic, and teratogenic properties (Mohamad Said et al., 2024; Neziri and Duranoğlu, 2024). Therefore, the removal of phenolic compounds from wastewater has become an important focus in environmental management and pollution control. Among various treatment methods, adsorption has gained attention due to its simplicity, cost-effectiveness, and ability to remove contaminants effectively without generating harmful by-products (Amri et al., 2024; Hafeez et al., 2024; Palapa et al., 2023a).

Adsorbents used in the adsorption process have many forms, both organic and inorganic have been widely reported. Many inorganic and organic adsorbents have been reported for pollutant removal applications; however, low-cost adsorbents with flexible adsorption capabilities, high chemical and thermal stability, and excellent reusability have emerged as promising candidates for sustainable and efficient use (Emilia et al., 2023; Ren et al., 2024). Carbon-based adsorbents are widely recognized for their selectivity, exceptional adsorption capacity, and robust thermal and chemical stability. Carbon-based adsorbents present a challenge in enhancing adsorption capacity while maintaining high regeneration capability (Tang et al., 2024; Wijaya and Yuliasari, 2023).

Recent studies have underscored the effectiveness of carbon-based adsorbents for pollutant removal. Liu et al. (2024) investigated biochar derived from eucalyptus waste, achieving an adsorption capacity of 172.5 mg/g for desulfurization purposes. Similarly, Correa-Navarro et al. (2024) examined biochar produced from fique bagasse, which demonstrated an adsorption capacity of 20.95 mg/g for butylparaben removal. Khorasani and Satvati (2024) utilized microcrystalline cellulose from walnut shells for iodine adsorption, reporting an adsorption capacity of

555.63 mg/g, with only a 17.45% reduction in capacity after six regeneration cycles. These findings suggest that carbon-based adsorbents are promising materials for the effective removal of pollutants from aqueous solutions.

This study aims to evaluate and compare the adsorption capabilities of rice husk biochar and microcrystalline cellulose for phenol removal. Through detailed characterization using XRD, FTIR, and nitrogen adsorption-desorption isotherms, this work explores the structural differences between BC and MC. Adsorption kinetics and isotherm models are investigated to understand the adsorption mechanism, while thermodynamic parameters provide insights into the nature and spontaneity of the adsorption process. Furthermore, reusability tests are conducted to assess the potential of BC and MC for repeated use in adsorption cycles. This comprehensive analysis is intended to highlight the strengths and limitations of BC and MC as adsorbents for phenol, ultimately contributing to the development of effective and sustainable phenol removal strategies.

2. EXPERIMENTAL SECTION

2.1 Chemicals and Instrumentations

Rice husk biochar (BC) was obtained from CV Buntara Karta Tani Yogyakarta and microcrystalline cellulose (MC) was purchased from Merck. Chemicals such as phenol (C_6H_5OH), distilled water (H_2O), 4-amino antipyrine ($C_{11}H_{13}N_3O$), cellulose, potassium hexacyanoferrate (III) ($K_3[Fe(CN)_6]$), sodium acetate buffer solution pH 10, hydrochloric acid (HCl), and sodium hydroxide (NaOH).

Characterization of materials was performed by XRD Rigaku Miniflex-600, FTIR Shimadzu Prestige-21 using the KBr method, and BET analysis using Quantachrome Micrometric 2020. The concentration of phenol was analyzed by UV-visible BioBase BK-UV 1800 PC spectrophotometer after complexation using 4-amino antipyrine, potassium hexacyanoferrate(III), and sodium acetate buffer solution pH 10 at 510 nm.

2.2 Procedure

2.2.1 Effect of Variation pH on Phenol Adsorption

20 mL of phenol with a concentration of 15 mg/L, was introduced into a 100 mL beaker. The pH was subsequently adjusted using NaOH and HCl solutions, targeting pH levels of 2, 3, 4, 5, 6, 7, 8, 9, 10, and 11. Following the complexation process, the initial absorbance for each pH level was measured using a UV-Vis spectrophotometer. A total of 0.02 grams of the adsorbent was introduced into the phenol solution and subjected to stirring for a duration of 2 hours. The separation procedure was conducted via centrifugation, and the resulting filtrate was quantified utilizing a UV-Vis spectrophotometer following the complexation process.

2.2.2 Effect of Contact Time, Concentration, and Temperature on Phenol Adsorption (Kinetic, Isotherm, and Thermodynamics Studies)

A solution of 15 mg/L phenol as much as 20 mL which has been inserted as much as 0.02g adsorbent then carried out the adsorption process with several tests. The variation of phenol adsorption time was carried out at 0, 5, 10, 15, 20, 30, 60, 90, 100, 120, 150, and 180 minutes. Concentration variations of 0 mg/L, 10 mg/L, 15 mg/L, 20 mg/L, 25 mg/L and 30 mg/L with temperature variations of 30°C, 40°C, 50°C, 60°C, and 70°C. After the adsorption process is complete, separate the adsorbent from the phenol solution. The complex solution was measured for absorbance value using a UV-Vis spectrophotometer. The kinetics study was studied from the adsorption time variation data while the isotherm & thermodynamic study was studied from the adsorption concentration and temperature variation data.

2.2.3 Reusability of Materials for Phenol Adsorption

The material reusability test begins with the desorption process first using distilled water assisted by an ultrasonic device for 15 minutes, then the adsorbent that has gone through the desorption process is inserted into 20 mL of phenol solution with a concentration of 15 mg/L. The mixture was stirred for 2 hours and the residual concentration was measured using a UV-Vis spectrophotometer. The adsorbent was dried and continued with the desorption process. The filtrate was then complexed and measured using a UV-Vis spectrophotometer. The adsorbent was then dried and reused in the next regeneration process.

3. RESULTS AND DISCUSSION

The XRD pattern depicting the BC and MC is presented in Figure 1. The BC exhibited a comprehensive diffraction pattern, characterized by a broadened maximum diffraction peak located at approximately 22° (002). The observed diffraction at (002) was ascribed to the elevated carbon content derived from rice husk (Palapa et al., 2023b). The observed peaks on the MC at angles of 15°, 22°, and 35° are associated with the 110, 200, and 004 crystal planes, respectively. The XRD pattern reveals the existence of polymorphous cellulose I, whereas the lack of the doublet crystal peak at 22° suggests the absence of type II cellulose. The XRD diffractogram pattern of the pure compound cellulose distinctly revealed significant findings. Nevertheless, it appears that the intensity of the diffraction peaks is relatively low. The observed diffraction peaks are attributed to the diffraction intensity associated with the amorphous component of the pure cellulose compound. The diffraction peaks exhibiting significant intensity in the vicinity of the 22° region are correlated with the diffraction intensity of the crystalline component of the pure cellulose compound (Debnath et al., 2022; Machmudah et al., 2025).

Figure 2 exhibits the FTIR spectra for BC and MC. The vibration peaks observed in BC and MC exhibit no significant difference, attributable to their shared composition as carbon-based materials; rather, it is the intensity of these vibration peaks that serves to differentiate the two. The absorption peak observed at 3330 cm^{-1} corresponds to the stretching vibration of the O–H bond found in native cellulose (Nayanajith et al., 2024). The absorption band observed at approximately 2900 cm^{-1} is likely associated with the symmetric stretching of the C–H bond in alkyl groups. The absorbance peak observed at 1640 cm^{-1} corresponds to the bending vibrations of the –OH groups associated with absorbed water, as well as the bending of the C=O bond present in aldehyde groups. The BC and MC showed

a peak at 1035 cm^{-1}, which was associated with the stretching vibration of C–O–C (Debnath et al., 2022).

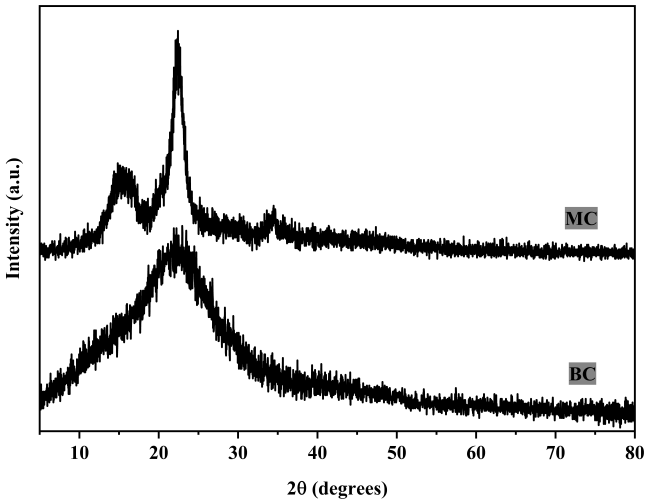

Figure 1. XRD Pattern of BC and MC

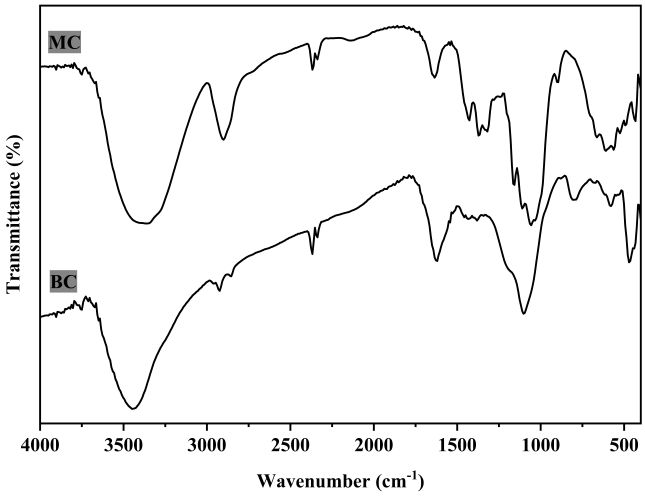

Figure 2. FTIR Spectra of BC and MC

The nitrogen isotherm adsorption-desorption of BC and MC materials is shown in Figure 3. The isotherms display the relationship between the volume of gas adsorbed and desorbed (in cc/g, STP) as a function of relative pressure (P/P_0). For both MC and BC, the isotherms exhibit a characteristic type IV pattern with a noticeable hysteresis loop, which is indicative of mesoporous materials. The presence of the hysteresis loop suggests that the materials possess a porous structure with a significant amount of mesopores (Wijaya and Yuliasari, 2023). This can be attributed to capillary condensation taking place within the mesopores at higher relative pressures. Overall, the differences in adsorption behavior between MC and BC can be linked to their distinct surface characteristics and pore structures, which play a crucial role in their efficiency as adsorbents for phenol removal in aqueous solutions.

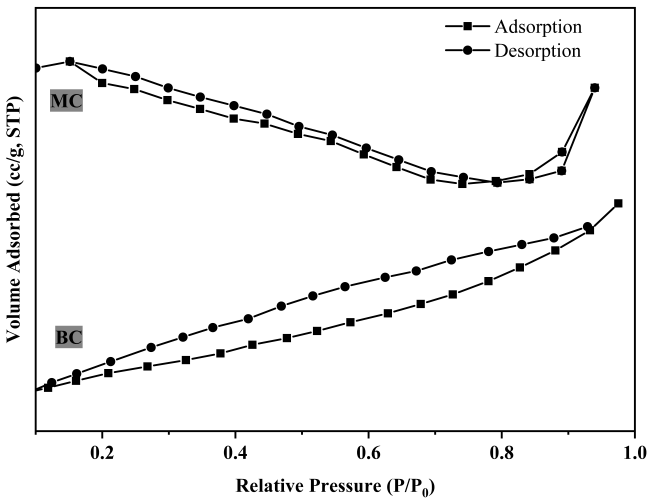

Figure 3. N_2 Isotherm Adsorption-desorption Profile of of BC and MC

Table 1. BET Data

Materials	Surface Area (m^2/g), BJH	Pore Size (nm), BJH	Pore Volume (cc/g), BJH
BC	30.60	3.56	0.04
MC	0.40	13.19	0.002

The data of the adsorption-desorption isotherm in Figure 3 was then calculated using the BJH (Barrett-Joyner-Halenda) method as shown in Table 1. The BC sample exhibits a notably higher surface area of 30.60 m^2/g, compared to the relatively low surface area of 0.40 m^2/g for the MC sample. This higher surface area of BC suggests that it offers more active sites for adsorption, making it potentially more effective as an adsorbent material. The pore size data also indicates a clear contrast between the two materials. MC shows a much larger average pore size of 13.19 nm, indicating the presence of macropores and large mesopores, while BC has a smaller average pore size of 3.56 nm, which suggests the dominance of mesopores. The larger pore size in MC may facilitate faster diffusion of adsorbates but may also limit its adsorption efficiency due to reduced surface area. BC shows a higher pore volume of 0.04 cc/g, indicating a greater capacity to accommodate adsorbates compared to the lower pore volume of 0.002 cc/g for MC. The combination of a larger surface area and higher pore volume in BC likely contributes to its enhanced adsorption characteristics.

Figure 4 illustrates the effect of pH on the adsorption capacity of phenol using BC and MC. For both BC and MC, the adsorption capacity increases as the pH rises from acidic to neutral conditions. At low pH (2–4), the adsorption capacity for both materials is relatively low, which can be attributed to the protonation of

Table 2. Adsorption Kinetic Models

Materials	Initial Concentration (mg/L)	Q_{eExp} (mg/g)	Pseudo First Order (PFO)			Pseudo Second Order (PSO)		
			Q_{eCalc} (mg/g)	R^2	k_1	Q_{eCalc} (mg/g)	R^2	k_2
BC	15.00	8.98	2.40	0.87	0.04	9.09	0.99	0.05
MC	10.00	3.62	1.68	0.90	0.03	3.80	0.99	0.04

Table 3. Adsorption Isotherm Models

Materials	T (K)	Langmuir			Freundlich		
		Q_{max} (mg/g)	k_L (mg/L)	R^2	n	k_F	R^2
BC	303	28.50	1.14	0.97	4.57	1.74	0.88
	313	23.04	0.58	0.99	9.02	1.87	0.92
	323	21.10	0.32	0.99	18.66	2.17	0.94
	333	24.80	0.21	0.99	18.11	2.45	0.89
	343	24.15	0.13	0.99	32.47	2.65	0.89
MC	303	6.93	0.05	0.99	0.41	13.87	0.97
	313	9.54	0.05	0.99	0.46	11.15	0.98
	323	13.25	0.04	0.99	0.50	10.50	0.98
	333	7.10	0.10	0.99	0.59	7.24	0.98
	343	8.11	0.11	0.99	0.66	4.39	0.99

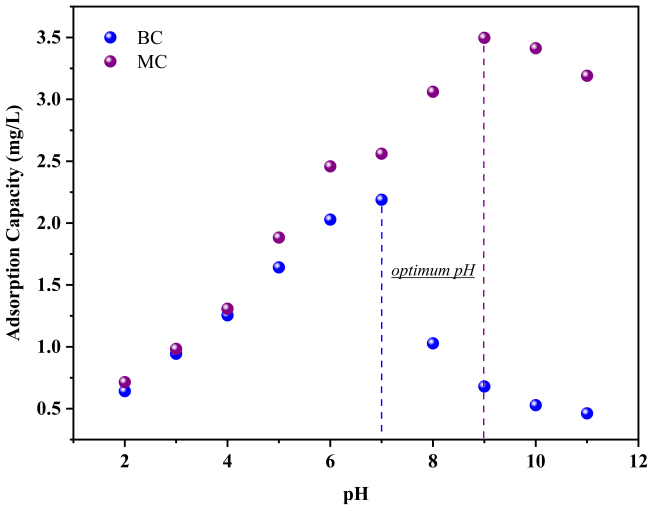

Figure 4. Effect of pH on Phenol Adsorption

phenol molecules and the positively charged surface of the adsorbents. This results in weaker interactions between the adsorbate and the adsorbent. As the pH increases, there is a noticeable rise in the adsorption capacity, with each material reaching its peak at an optimum pH. The optimum pH for BC is around 7, while for MC, it is closer to pH 9. At these points, the surface of the adsorbents is likely neutral or slightly negatively charged, allowing for stronger interactions with the phenol molecules, which enhances adsorption efficiency. Beyond the optimum pH, the adsorption capacity for both BC and MC decreases. This decline can be attributed to the deprotonation of phenol and increased competition between phenolate anions and hydroxide ions (OH^-) for active sites on the adsorbent surfaces, reducing the overall adsorption effectiveness.

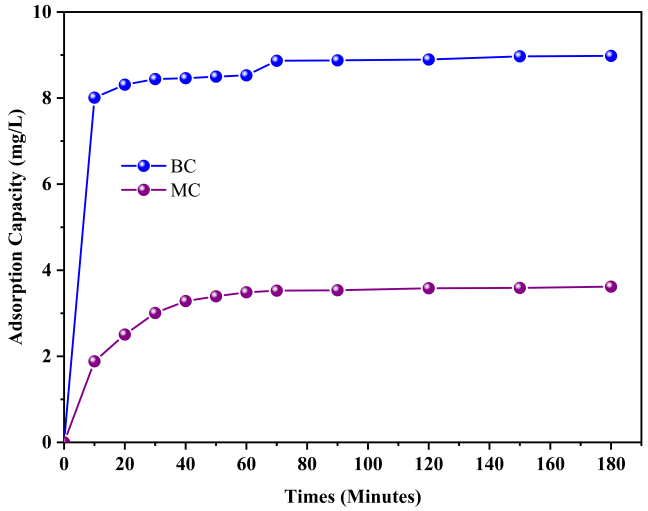

Figure 5. Effect of Contact Times on Phenol Adsorption

The effect of contact time on the adsorption capacity of phenol using BC and MC is shown in Figure 5. It can be observed that the adsorption capacity for both adsorbents initially increases rapidly, indicating fast adsorption within the first 20 minutes. However, BC exhibits a much higher adsorption capacity, reaching around 8 mg/L, whereas MC plateaus at approximately 3 mg/L. After 40 minutes, both adsorbents approach equilibrium, with minimal change in adsorption capacity beyond this point.

Table 4. Thermodynamic Adsorption (C_0: 30 mg/L)

Materials	T (K)	Q_e (mg/g)	ΔH (kJ/mol)	ΔS (J/mol.K)	ΔG (kJ/mol)
BC	303	24.07	25.06	0.09	-3.27
	313	25.11			-4.21
	323	26.13			-5.14
	333	27.05			-6.08
	343	28.03			-7.01
MC	303	15.21	1.46	0.01	-0.06
	313	15.40			-0.11
	323	15.50			-0.16
	333	15.52			-0.21
	343	15.78			-0.26

These results suggest that BC has a significantly higher efficiency in phenol adsorption compared to MC, potentially due to differences in surface properties or porosity.

Table 2 presents the adsorption kinetic parameters for phenol adsorption onto BC and MC using both the PSO and PFO models. The experimental adsorption capacities for BC and MC are 8.98 mg/g and 3.62 mg/g, respectively. The PSO model shows a better fit for both materials, as indicated by the higher R^2 values (0.99 for both BC and MC) compared to the PFO model, which has R^2 values of 0.87 for BC and 0.90 for MC. This suggests that the adsorption process is more accurately described by the PSO model, indicating that chemisorption may be the rate-limiting step (Tang et al., 2024; Zhu et al., 2024). The Q_{eCalc} values from the PSO model are also closer to the experimental values, reinforcing that this model better predicts the adsorption capacity.

Table 3 shows the adsorption isotherm parameters for phenol adsorption onto BC and MC at different temperatures, analyzed using the Langmuir and Freundlich models. For the Langmuir model, the maximum adsorption capacity for BC is highest at 303 K (28.50 mg/g) and decreases slightly with increasing temperature, indicating that higher temperatures may reduce BC's adsorption capacity. Similarly, MC shows its highest adsorption capacity at 323 K (13.25 mg/g). The high R^2 values indicate a good fit for the Langmuir model, suggesting monolayer adsorption on a homogenous surface for both adsorbents (Wu et al., 2025).

In the Freundlich model, the parameter n indicates adsorption favorability. For BC, n values increase significantly with temperature, suggesting enhanced adsorption affinity. In contrast, n values for MC are relatively low and show minor variation, implying less favorable adsorption compared to BC. However, the R^2 values for the Freundlich model are generally lower than those for the Langmuir model, indicating that the Langmuir model provides a better fit for both BC and MC. This result implies that adsorption onto both materials is more likely to occur as a monolayer rather than multilayer adsorption.

The thermodynamic parameters presented in Table 4 provide insights into the adsorption process of phenol onto BC and MC materials. For BC, the Q_e values increase with temperature, ranging from 24.07 mg/g at 303 K to 28.03 mg/g at 343 K. This increase suggests that the adsorption of phenol onto BC is endothermic, as higher temperatures enhance the adsorption capacity. The positive value of ΔH (25.06 kJ/mol) confirms the endothermic nature of the process, indicating that energy input is required for phenol molecules to be adsorbed onto the BC surface. The positive entropy change (ΔS=0.09 J/mol.K) suggests an increase in randomness at the solid-liquid interface during adsorption, potentially due to structural changes in the phenol or adsorbent. The negative ΔG values, which decrease with rising temperature (from -3.27 kJ/mol at 303 K to -7.01 kJ/mol at 343 K), imply that the adsorption is spontaneous and becomes more favorable at higher temperatures (Ton-That et al., 2024; Xian et al., 2024).

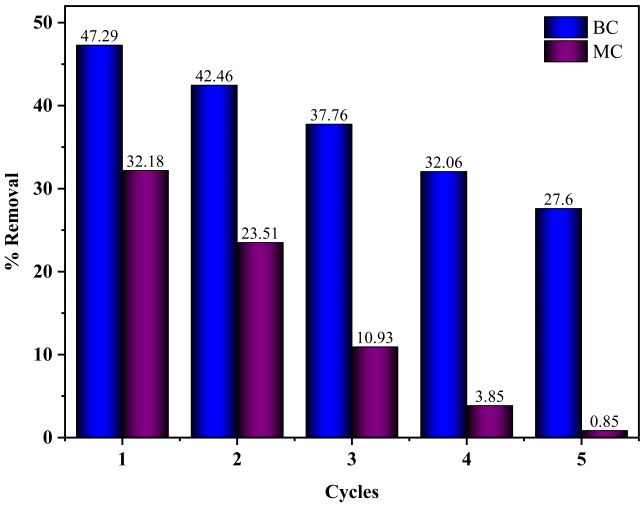

Figure 6. Reusability of BC and BC on Phenol Adsorption

In the case of MC, the Q_e values show only slight changes with increasing temperature, from 15.21 mg/g at 303 K to 15.78 mg/g at 343 K. This limited increase in Q_e suggests that temperature has a minimal effect on the adsorption capacity of MC,

indicating a less pronounced endothermic process. The ΔH value for MC (1.46 kJ/mol) is considerably lower than that for BC, which aligns with the observed low sensitivity to temperature. The small positive ΔS value (0.01 J/mol.K) implies minimal disorder changes, while the nearly constant, slightly negative ΔG values (ranging from -0.06 kJ/mol to -0.26 kJ/mol) indicate that the adsorption onto MC is only marginally spontaneous and temperature-independent (Kosale et al., 2024; Normah et al., 2024). The thermodynamic data suggest that BC is a more effective adsorbent for phenol due to its higher endothermic enthalpy and greater spontaneity with temperature increase, while MC demonstrates a weaker adsorption affinity with minimal temperature dependence.

Figure 6 illustrates the reusability performance of BC and MC materials for phenol adsorption over five consecutive cycles. For both materials, there is a noticeable decrease in removal efficiency with each cycle, indicating a reduction in adsorption capacity upon reuse. In the first cycle, BC achieves a higher removal efficiency (47.29%) compared to MC (32.18%), demonstrating better initial adsorption performance. As the cycles progress, the efficiency of BC decreases steadily, reaching 27.6% by the fifth cycle. In contrast, MC shows a more rapid decline, dropping to only 0.85% in the fifth cycle. These results suggest that BC has greater reusability potential for phenol adsorption than MC, retaining more of its adsorption capability across multiple cycles.

4. CONCLUSIONS

This study concludes that BC, with its higher surface area, crystallinity, and endothermic adsorption characteristics, is a more effective adsorbent for phenol removal compared to MC. The adsorption process on both BC and MC follows the PSO model, indicating chemisorption as the rate-limiting step, and fits well with the Langmuir isotherm, suggesting monolayer adsorption. Thermodynamic analysis further confirms the endothermic and spontaneous nature of phenol adsorption on BC, with adsorption efficiency increasing at higher temperatures. BC also demonstrates superior reusability, maintaining substantial adsorption capacity over multiple cycles, in contrast to the rapid decline in adsorption efficiency observed for MC. These findings suggest that BC has promising potential for practical applications in phenol removal from wastewater, especially where reusability and efficiency are essential.

5. ACKNOWLEDGEMENT

The authors extend their gratitude to the “Research Center for Inorganic Materials and Coordination Complexes” at Universitas Sriwijaya for their valuable contributions through discussions, support, and instrumental analysis provided throughout this research.

REFERENCES

Amri, A., S. Wibiyan, A. Wijaya, N. Ahmad, R. Mohadi, and A. Lesbani (2024). Efficient Adsorption of Methylene Blue Dye Using Ni/Al Layered Double Hydroxide-Graphene Oxide Composite. *Bulletin of Chemical Reaction Engineering & Catalysis*, **19**(2); 181–189

Correa-Navarro, Y. M., J. D. Rivera-Giraldo, and J. D. Murcia-García (2024). Isotherm and Kinetic Data for Adsorption of Butylparaben onto Biochars Derived from *Fique bagasse. Data in Brief*, **In Press**; 111113

Debnath, B., P. Duarah, D. Haldar, and M. K. Purkait (2022). Improving the Properties of Corn Starch Films for Application as Packaging Material via Reinforcement with Microcrystalline Cellulose Synthesized from Elephant Grass. *Food Packaging and Shelf Life*, **34**; 100937

Emilia, D., Y. M. Hakim, and R. Mohadi (2023). Mangan Oxide-Assisted in Biochar Improvement and Application in Malachite Green Removal. *Indonesian Journal of Material Research*, **1**(2); 35–43

Hafeez, S., A. Ishaq, A. Intisar, T. Mahmood, M. I. Din, E. Ahmed, M. R. Tariq, and M. A. Abid (2024). Predictive Modeling for the Adsorptive and Photocatalytic Removal of Phenolic Contaminants from Water Using Artificial Neural Networks. *Heliyon*, **10**(19); e37951

Khorasani, A. C. and P. R. Satvati (2024). Reusable Cellulose-Based Biosorbents for Efficient Iodine Adsorption by Economic Microcrystalline Cellulose Production from Walnut Shell. *International Journal of Biological Macromolecules*, **256**; 128432

Kosale, D., V. K. Singh, and C. Thakur (2024). Comparative Adsorption of Cationic and Anionic Dye by Using Non-Activated Black Plum Seed Biochar for Aquatic Phase: Isotherm, Kinetic and Thermodynamic Studies. *Industrial Crops and Products*, **215**; 118609

Liu, Q., Q. Chang, X. Liao, Y. Jiang, X. Lyu, Q. Zhao, J. Diao, X. Wang, X. Huang, and S. Lyu (2024). Adsorption Desulphurization Performance of Biochar That Derived from *Eucalyptus* Waste. *Powder Technology*, **448**; 120322

Machmudah, S., Wahyudiono, P. N. Trisanti, H. Setyawan, S. Madhania, K. Sambodho, S. Winardi, T. Adschiri, and M. Goto (2025). Hydrothermal Alkaline Treatment of Lignocellulosic Biomass for Microcrystalline Cellulose Generation at Subcritical Water. *South African Journal of Chemical Engineering*, **51**; 45–56

Mohamad Said, K. A., M. P. M. Subasinghe, M. R. Rahman, I. Yakub, and S. Hamdan (2024). Magnetic Driven Particle Migration in PES Membrane for Phenol Adsorption Study: Isotherm and Kinetic Model Perspective. *Chemical Physics Impact*, **9**; 100766

Nayanajith, M. H., C. J. Narangoda, A. I. Ratnayake, L. Karunanayake, and D. A. S. Amarasinghe (2024). Enhancement of Mechanical Properties of Natural Rubber Latex Sheets by Incorporating Allyl-Modified Microcrystalline Cellulose (AMCC). *Materials Today Communications*, **41**; 110873

Neziri, E. and D. Duranoğlu (2024). Kinetic, Equilibrium, and Thermodynamic Aspects of Phenol Adsorption onto Acrylonitrile-Divinylbenzene Copolymer. *Science of the Total Environment*, **954**; 1–10

Normah, N., N. Adhiyanti, R. J. Sayeri, and A. Wijaya (2024). Efficient Adsorption of Cr(VI) from Aqueous Solutions Using Composites. *Indonesian Journal of Material Research*, **2**(2); 32–39

Palapa, N. R., A. Wijaya, N. Ahmad, A. Amri, R. Mohadi, and A. Lesbani (2023a). Activated Hydrochar Prepared from Longan Fruit (*Dimocarpus longan* Lour.) Peel via Hydrothermal Carbonization-NaOH Activation for Cationic Dyes Removal. *Science and Technology Indonesia*, **8**(3); 461–470

Palapa, N. R., A. Wijaya, P. M. S. B. N. Siregar, A. Amri, N. Ahmad, T. Taher, and A. Lesbani (2023b). Adsorption of Fe(II) by Layered Double Hydroxide Composite with Carbon-Based Material (Biochar and Graphite): Reusability and Thermodynamic Properties. *Indonesian Journal of Chemistry*, **23**(1); 101–112

Ren, J., Y. Zhang, H. Wang, X. Huang, X. Jin, K. Zhang, R. Li, K. Yang, Y. Yue, L. Deng, and D. Che (2024). Adsorption of Dibenzofuran by Modified Biochar Derived from Microwave Gasification: Impact Factors and Adsorption Mechanism. *Journal of Analytical and Applied Pyrolysis*, **183**; 106831

Tang, G., H. Mo, L. Gao, Y. Chen, and X. Zhou (2024). Adsorption of Crystal Violet from Wastewater Using Alkaline-Modified Pomelo Peel-Derived Biochar. *Journal of Water Process Engineering*, **68**; 106334

Ton-That, L., T. P. T. Nguyen, B. N. Duong, D. K. Nguyen, N. A. Nguyen, T. H. Ho, and V. P. Dinh (2024). Insights into Pb(II) Adsorption Mechanisms Using Jackfruit Peel Biochar Activated by a Hydrothermal Method Toward Heavy Metal Removal from Wastewater. *Biochemical Engineering Journal*, **212**; 109525

Wijaya, A. and N. Yuliasari (2023). Biochar Derived from Rice Husk as Effective Adsorbent for the Removal Congo Red and Procion Red MX-5B Dyes. *Indonesian Journal of Material Research*, **1**(1); 1–7

Wu, W., J. Liu, G. Zhang, Y. Wang, C. Wu, G. Li, and Y. Zhao (2025). Adsorption of CO_2 by Sludge/Bamboo Shoot Shell Hybrid Biochar Prepared by a Single-Step K_2CO_3 Activation. *Fuel*, **381**(PC); 133555

Wu, X., C. Cai, Q. Cen, G. Fu, X. Lu, H. Zheng, Q. Zhang, X. Cui, and Y. Liu (2024). Efficient Catalytic Removal of Phenolic Pollutants by Laccase from *Coriolopsis gallica*: Binding Interaction and Polymerization Mechanism. *International Journal of Biological Macromolecules*, **279**(P3); 135272

Xian, B., W. Tang, D. Xiang, C. Rao, X. Liu, F. Fang, F. Chu, and T. Fang (2024). Preparation of Organic Potassium Salts Modified Microalgae Biochar and Its High-Efficient Removal of Tetracycline Hydrochloride from Water: Activation Mechanism and Adsorption Mechanism. *Journal of Water Process Engineering*, **67**(July); 106122

Zhu, C., J. Zhang, G. Huang, and D. Z. Zhu (2024). UV-Modified Biochar-Bacillus Subtilis Composite: An Effective Method for Enhancing Cd(II) Adsorption from Water. *Biochemical Engineering Journal*, **212**(July); 109527

Zubir, A., E. Normaya, N. H. Zuhaidi, P. S. Goh, M. B. M. Piah, M. W. Ismail, P. L. Show, A. F. Ismail, and M. N. Ahmad (2024). Optimization and Mechanistic Insight of Phenol Removal Using an Effective Green Kaolin Adsorbent Through Experimental and Computational Approaches. *Journal of Molecular Structure*, **1318**(P2); 139219

